

**PREPARATION AND CHARACTERIZATION OF  
EPOXIDIZED SOYBEAN OIL BASED THERMOSET,  
BLENDS AND NANOCOMPOSITES**

**by**

**TAN SEAH GUAN**

**Thesis submitted in fulfillment of the requirements**

**for the degree of**

**Doctor of Philosophy**

**FEBRUARY 2013**

## ACKNOWLEDGEMENT

First and foremost, I would like to express my heartfelt gratitude and appreciation to School of Materials and Mineral Resources Engineering, USM for providing me with an opportunity to pursue my postgraduate study. Also, I wish to extend my thanks to USM for granting me a postgraduate research grant (USM-RU-PRGS, Grant Number 1001/PBAHAN/8045001) that enabled me to conduct lots of my research works and achieve the research objectives. Besides, I also gratefully acknowledge the Ministry of Science, Technology and Innovation, Malaysia (MOSTI) for the National Science Foundation (NSF) fellowship.

Apart from that, I am deeply indebted to my project supervisor, Assoc. Prof. Dr. Chow Wen Shyang, and co-supervisor, Assoc. Prof. Dr. Zulkifli Ahmad, for their valuable suggestions, assistance and guidance in implementing my research project. I cannot thank them more for the time and effort they spent with me for the discussion, supervision in thesis writing and experience sharing. Also, I would like to extend my sincerest thanks and appreciation to Dr. Chow for giving me the opportunities to join various conferences to present my research work. Furthermore, I am very thankful to Prof. Sudesh Kumar and his students, Mr. Chia Kim Hou and Ms. Lau Nyok Sean, from School of Biological Science, USM for their generous help in guiding me all the way to perform the microbial identification work in their research lab. I also wish to thank Prof. Sudesh for his willingness to collaborate with us on this project.

In addition, I would like to express my great gratefulness to all the lecturers and technicians in School of Materials and Mineral Resources Engineering, USM. The contributions of the professional practitioner with whom I have worked with are indispensable. Last, but certainly not least, I wish to thank my family and friends for their continual encouragement, support and constructive criticism.

## TABLE OF CONTENTS

	<b>Page</b>
<b>Acknowledgement</b>	ii
<b>Table of Contents</b>	iii
<b>List of Tables</b>	vii
<b>List of Figures</b>	ix
<b>List of Abbreviations</b>	xiv
<b>List of Symbols</b>	xv
<b>Abstrak</b>	xvii
<b>Abstract</b>	xix
<b>CHAPTER 1 INTRODUCTION</b>	
1.1 Research Background	1
1.2 Problem Statement	3
1.3 Hypothesis and Motivation	5
1.4 Research Objectives	5
1.5 Research Scopes	6
1.6 Structure of Thesis	6
<b>CHAPTER 2 LITERATURE REVIEW</b>	
2.1 Vegetable Oils	8
2.1.1 Types of Vegetable Oils	9
2.1.2 Vegetable Oil Producers	12
2.1.3 Global Use of Vegetable Oils	13
2.2 Epoxidized Soybean Oil	13
2.2.1 Curing Reaction of Epoxidized Soybean Oil	15
2.2.2 Properties of Epoxidized Soybean Oil Thermoset	20
2.2.3 Recent Development of Epoxidized Soybean Oil	22
2.2.3.1 Epoxidized Soybean Oil-based Thermoset Blends	23
2.2.3.2 Epoxidized Soybean Oil-based Composites	27

2.3	Curing Agents	30
2.3.1	Anhydrides	32
2.3.1.1	Methylhexahydrophthalic Anhydride	34
2.4	Catalysts	35
2.4.1	2-Ethyl-4-Methylimidazoles	36
2.4.2	Tetraethylammonium Bromide	37
2.5	Curing Kinetics of Thermosets	37
2.5.1	Kinetic Studies of Epoxidized Vegetable Oils	38
2.5.2	Cure Kinetic Models	39
2.6	Fracture Toughness	41
2.6.1	Linear Elastic Fracture Mechanics	43
2.6.2	Essential Work of Fracture	45
2.7	Water Absorption	49
2.7.1	Diffusion and Fick's Law	50
2.7.2	Water Absorption of Thermosets	52
2.8	Biodegradation	53
2.8.1	Biodegradation Studies of Epoxidized Vegetable Oils	54
2.8.2	Isolation of Polymer Degradation Microorganisms	55

### **CHAPTER 3 MATERIALS AND METHODS**

3.1	Materials	58
3.1.1	Epoxidized Soybean Oil	58
3.1.2	Epoxy Resin	59
3.1.3	Curing Agent	59
3.1.4	Catalysts	60
3.1.5	Filler	61
3.2	Sample Preparation for Cure Kinetics Studies	62
3.3	Curing Kinetics Studies using FTIR	62
3.4	Materials Preparation	64
3.4.1	Mixing	64
3.4.1.1	ESO Thermosets	64
3.4.1.2	ESO/DGEBA Blends	65
3.4.1.3	ESO/OMMT Nanocomposites	66

3.4.2	Thermal Curing	66
3.5	Materials Characterization	67
3.5.1	Physical Testing	67
3.5.1.1	Hardness Measurement	67
3.5.1.2	Density Measurement	67
3.5.2	Mechanical Testing	68
3.5.2.1	Fracture Toughness Measurement	68
3.5.2.2	Tensile Test	70
3.5.3	Thermal Testing	70
3.5.3.1	Dynamic Mechanical Analysis	70
3.5.3.2	Differential Scanning Calorimetry	71
3.5.3.3	Thermogravimetry Analysis	71
3.5.4	Morphological Characterization	72
3.5.4.1	Scanning Electron Microscopy	72
3.5.4.2	Atomic Force Microscopy	72
3.5.4.3	Transmission Electron Microscopy	73
3.5.5	Gel Content Measurement	73
3.5.6	X-ray Diffraction	73
3.5.7	Water Absorption Studies	74
3.5.8	Degradation Study	75
3.5.8.1	Soil Burial Test	75
3.5.8.2	Weight Loss Measurement	75
3.5.8.3	Isolation and Identification of Bacterial Strain	76

## **CHAPTER 4 RESULTS AND DISCUSSION**

4.1	FTIR and Cure Kinetic Studies of ESO	77
4.1.1	FTIR Characterization	77
4.1.2	Reaction Kinetics	84
4.1.3	Analysis of Reaction Kinetics	88
4.1.4	Activation Energy	93
4.1.5	Cure Kinetic Models	96

4.2	Properties of ESO Thermosets	99
4.2.1	Thermal Properties	99
4.2.1.1	Dynamic Mechanical Analysis	99
4.2.1.2	Differential Scanning Calorimetry Analysis	104
4.2.1.3	Thermogravimetry Analysis	108
4.2.2	Fracture Toughness	112
4.2.2.1	Essential Work of Fracture	112
4.2.2.2	Linear Elastic Fracture Mechanics	114
4.2.2.3	LEFM and EWF Fracture Characterization	120
4.2.2.4	Morphology Characterization	122
4.2.3	Physical Properties	127
4.2.3.1	Hardness	127
4.2.3.2	Density	128
4.2.4	Kinetics of Water Absorption	128
4.2.5	Comparison Analysis	132
4.3	ESO/DGEBA Blends	133
4.3.1	Mechanical Properties	133
4.3.2	Thermal Properties	141
4.4	ESO/OMMT Nanocomposites	146
4.4.1	Mechanical Properties	146
4.4.2	Thermal Properties	152
4.5	Biodegradability of ESO Thermoset	160
4.5.1	Weight Changes and Physical Appearance	160
4.5.2	Morphological Properties	166
4.5.3	Isolation and Identification of Bacterial Strains	167
<b>CHAPTER 5 CONCLUSION</b>		
5.1	Conclusion	170
5.2	Recommendations for Future Studies	173
<b>REFERENCES</b>		172
<b>APPENDICES</b>		

## LIST OF TABLES

		<b>Page</b>
Table 2.1	Different epoxidation process of various types of vegetable oils, and their efficiency, selectivity and epoxy content	10
Table 2.2	List of fatty acid profiles in some vegetable oils	11
Table 2.3	Thermal and mechanical properties of ESO/petroleum-based epoxy blends	26
Table 2.4	Mechanical and thermal properties of ESO composites	31
Table 2.5	Commercially used anhydride curing agents	33
Table 2.6	Geometry and $K_{IC}$ for different fracture mechanics specimens	47
Table 3.1	Typical properties of ESO resin	58
Table 3.2	Typical properties of DGEBA resin	59
Table 3.3	Typical properties of MHHPA curing agent	60
Table 3.4	Typical properties of OMMT clay	61
Table 3.5	Materials designation and composition of ESO samples	62
Table 3.6	Materials designation and composition of EMI-catalyzed ESO thermosets	64
Table 3.7	Materials designation and composition of TEBA-catalyzed ESO thermosets	65
Table 3.8	Materials designation and composition of ESO/DGEBA blends	65
Table 3.9	Materials designation and composition of ESO/OMMT nanocomposites	66
Table 4.1	The normalized FTIR peak areas of ESO/catalyst mixtures	79
Table 4.2	FTIR peak assignment for ESO/MHHPA systems	81
Table 4.3	Kinetic and diffusion parameters of EMI-catalyzed ESO/MHHPA systems	91

Table 4.4	Kinetic and diffusion parameters of TEAB-catalyzed ESO/MHHPA systems	90
Table 4.5	Thermal properties of ESO thermosets determined from DMA	101
Table 4.6	Gel content of ESO thermosets	103
Table 4.7	Thermal properties of ESO thermosets determined from DSC	106
Table 4.8	Thermal characteristics of ESO thermosets from TGA	111
Table 4.9	The specific essential work of fracture and the specific plastic fracture work of ESO thermosets	113
Table 4.10	Physical properties of ESO thermosets	127
Table 4.11	Maximum water uptake ( $M_m$ ) and diffusion coefficient ( $D$ ) of ESO thermoset	131
Table 4.12	Thermo-mechanical properties of thermosets based on ESO	132
Table 4.13	Mechanical and physical properties of ESO and ESO/DGEBA blends	134
Table 4.14	Thermal characteristics of ESO and ESO/DGEBA blends recorded from TGA characterization	145
Table 4.15	Mechanical and physical properties of ESO and ESO/OMMT nanocomposites	147
Table 4.16	Thermal characteristics of ESO and ESO/OMMT nanocomposites recorded from TGA characterization	159

## LIST OF FIGURES

	<b>Page</b>	
Figure 2.1	Typical chemical structure of vegetable oils	8
Figure 2.2	Global vegetable oil consumption	11
Figure 2.3	Structure of soybean oil and its substituted fatty acids	14
Figure 2.4	Curing mechanism of ESO resin with t-amines and anhydrides	15
Figure 2.5	Schematic represents the cationic photopolymerization mechanism of ESO in the presence of onium cationic photoinitiator	16
Figure 2.6	Thermal induced ring-opening cationic polymerization of internal epoxies in ESO initiated by BQH thermal latent initiator	17
Figure 2.7	Schematic curing mechanism of ESO/maleic anhydride reaction	19
Figure 2.8	Model of an elliptical crack of length $2a$ in a uniformly loaded infinite plate	44
Figure 2.9	The schematic diagrams displaying the fracture zones: (a) Inner fracture process zone (IFPZ) and outer process dissipation zone (OPDZ) and (b) the data reduction method of the EWF	48
Figure 2.10	General mechanisms of plastics biodegradation	54
Figure 2.11	Schematic drawing of PCR cycle. (1) Denaturation, (2) Annealing, (3) Elongation, (4) The first cycle is complete	57
Figure 3.1	Chemical structure of ESO resin	58
Figure 3.2	Chemical structure of DGEBA resin	59
Figure 3.3	Chemical structure of MHPA curing agent	60
Figure 3.4	Chemical structures of (a) EMI catalyst, and (b) TEAB catalyst	61
Figure 3.5	Silicone rubber mould for casting of ESO thermosetting materials	67

Figure 3.6	Schematic diagrams of SENT and DENT samples	69
Figure 3.7	ESO samples for the tensile test	70
Figure 4.1	FTIR spectra representing the ring opening of MHPA curing agent with EMI catalyst (Temp: 80°C)	78
Figure 4.2	FTIR spectra representing the ring opening of MHPA curing agent with TEAB catalyst (Temp: 80°C)	78
Figure 4.3	FTIR spectra of ESO/MHPA systems cured at 140°C	81
Figure 4.4	Proposed initiation and propagation mechanisms of EMI-catalyzed ESO thermosets	82
Figure 4.5	Proposed initiation and propagation mechanisms of TEAB-catalyzed ESO thermosets	83
Figure 4.6	Plot of degree of conversion as a function of cure time for (a) ES_0.5I, (b) ES_1.0I, (c) ES_1.5I and (d) ES_2.0I cured at different temperatures	85
Figure 4.7	Plot of degree of conversion as a function of cure time for (a) ES_0.5A, (b) ES_1.0A, (c) ES_1.5A and (d) ES_2.0A cured at different temperatures	85
Figure 4.8	Comparison of experimental data with Kamal's model for reaction rate versus degree of conversion of (a) ES_0.5I, (b) ES_1.0I, (c) ES_1.5I, and (d) ES_2.0I cured at different temperature	86
Figure 4.9	Comparison of experimental data with Kamal's model for reaction rate versus degree of conversion of (a) ES_0.5A, (b) ES_1.0A, (c) ES_1.5A, and (d) ES_2.0A cured at different temperature	86
Figure 4.10	Arrhenius-type plot for rate constant of (a) ES_0.5I, (b) ES_1.0I, (c) ES_1.5I, and (d) ES_2.0I	94
Figure 4.11	Arrhenius-type plot of rate constant of (a) ES_0.5A, (b) ES_1.0A, (c) ES_1.5A and (d) ES_2.0A	94
Figure 4.12	Effect of EMI catalyst content on the storage modulus ( $E'$ ) and $\tan \delta$ of the ESO thermosets	100
Figure 4.13	Effect of TEAB catalyst content on the storage modulus ( $E'$ ) and $\tan \delta$ of the ESO thermosets	100
Figure 4.14	DSC heating thermograms of EMI-catalyzed ESO thermosets	105

Figure 4.15	DSC heating thermograms of TEAB-catalyzed ESO thermosets	106
Figure 4.16	(a) TGA and (b) DTG curves of EMI-catalyzed ESO thermosets	109
Figure 4.17	(a) TGA and (b) DTG curves of TEAB-catalyzed ESO thermosets	110
Figure 4.18	Force versus displacement curves for (a) EMI-catalyzed ESO thermoset; (b) TEAB-catalyzed ESO thermosets	115
Figure 4.19	Single-edge notched tensile fracture toughness of ESO thermosets	115
Figure 4.20	Double-edge notched tensile fracture toughness of ESO thermosets	116
Figure 4.21	Correlation of fracture toughness and crosslink density for EMI and TEAB-catalyzed ESO thermosets	118
Figure 4.22	Photographs of ESO thermoset showing the ligament yielding	121
Figure 4.23	SEM micrographs of the fractured surface of (a) ES_0.3I, (b) ES_0.4I, (c) ES_0.5I, (d) ES_0.6I, (e) ES_0.7I, (f) ES_0.8I, (g) ES_0.9I, (h) ES_1.0I, (i) ES_1.5I, (j) ES_2.0I	123
Figure 4.24	SEM micrographs of the fractured surface of (a) ES_0.3A, (b) ES_0.4A, (c) ES_0.5A, (d) ES_0.6A, (e) ES_0.7A, (f) ES_0.8A, (g) ES_0.9A, (h) ES_1.0A, (i) ES_1.5A, (j) ES_2.0A	124
Figure 4.25	SEM micrographs of fractured surface of (a) ES_0.3I, (b) ES_0.5I, (c) ES_1.0I, (d) ES_2.0I at high magnification	125
Figure 4.26	Effect of EMI catalyst content on water uptake of ESO thermoset	129
Figure 4.27	Effect of TEAB catalyst content on water uptake of ESO thermoset	129
Figure 4.28	Experimental and calculated tensile modulus of ESO/DGEBA blends	135
Figure 4.29	SEM micrographs taken for the polished surface of (a) ESO, (b) DGEBA, (c) ESO/DGEBA (80/20), (d) ESO/DGEBA (60/40)	136
Figure 4.30	Topography (left) and phase contrast (right) AFM images taken for the polished surface of (a) ESO, (b) DGEBA, (c) ESO/DGEBA (80/20), (d) ESO/DGEBA (60/40)	137

Figure 4.31	TEM micrographs of osmium oxide strained ESO/DGEBA (60/40) blends at (a) 25000X magnification and (b) 80000X magnification	138
Figure 4.32	SEM micrographs taken fro the fractured surface of (a) ESO, (b) ESO/DGEBA (90/10), (c) ESO/DGEBA (80/20), (d) ESO/DGEBA (70/30), (e) ESO/DGEBA (60/40), (f) ESO/DGEBA (50/50)	140
Figure 4.33	Storage modulus and $\tan \delta$ curves of ESO and ESO/DGEBA blends	141
Figure 4.34	DSC thermograms registered for cured ESO and ESO/DGEBA blends	143
Figure 4.35	(a) TGA and (b) DTG curves of ESO and ESO/DGEBA blends	144
Figure 4.36	XRD spectra of ESO and ESO/OMMT nanocomposites	148
Figure 4.37	TEM micrographs of ESO/OMMT nanocomposites at (a) low magnification (4000X) and (b) at high magnification (63000X)	149
Figure 4.38	SEM micrographs taken for the fractured surface of (a) ESO, (b) ESO/OMMT_1, (c) ESO/OMMT_2, (d) ESO/OMMT_3, (e) ESO/OMMT_4, (f) ESO/OMMT_5	151
Figure 4.39	Storage modulus and $\tan \delta$ curves of ESO and ESO/OMMT nanocomposites	153
Figure 4.40	DSC thermograms registered for cured ESO and ESO/OMMT nanocomposites	154
Figure 4.41	The possible catalytic curing reaction of ESO resin by the MHPA	156
Figure 4.42	(a) TGA curves of ESO and ESO/OMMT nanocomposites	157
	(b) DTG curves of ESO and ESO/OMMT nanocomposites	158
Figure 4.43	Percentage of weight loss of the ESO thermosets as a function of soil buried time	161
Figure 4.44	Photographs of soil-buried ESO thermosets (a) ES_0.5I, (b) ES_1.0I, (c) ES_1.5I, and (d) ES_2.0I	163
Figure 4.45	Representative surface morphology of ESO thermoset (control sample)	164
Figure 4.46	SEM micrographs taken from the surfaces of the ES_0.5I thermoset after being soil-buried for (a) 2 months and (b) 4 months	164

Figure 4.47	SEM micrographs taken from the surfaces of the ES_1.0I thermoset after being soil-buried for (a) 2 months, (b) 4 months, (c) 6 months and (d) 8 months	165
Figure 4.48	SEM micrographs taken from the surfaces of the ES_1.5I thermoset after being soil-buried for (a) 2 months, (b) 4 months, (c) 6 months and (d) 8 months	165
Figure 4.49	SEM micrographs taken from the surfaces of the ES_2.0I thermoset after being soil-buried for (a) 2 months, (b) 4 months, (c) 6 months and (d) 8 months	166
Figure 4.50	Photographs of the isolated bacterial strains placed on the agar plates: (a) Dilution with low concentration of bacteria strain, and (b) dilution with high concentration of bacterial strain	167
Figure 4.51	Ethidium bromide-stained agarose gel electrophoresis of polymerase chain reaction (PCR) products for the 16 isolates	168

## LIST OF ABBREVIATIONS

AFM	Atomic Force Microscopy
ASTM	American Society for Testing and Materials
DENT	Double Edge Notched Tensile
DGEBA	Diglycidyl Ether of Bisphenol-A
DMA	Dynamic Mechanical Analysis
DSC	Differential Scanning Calorimetry
DTG	Differential Thermal Gravimetry
EMI	2-Ethyl-4-Methylimidazole
ESO	Epoxidized Soybean Oil
EVO	Epoxidized Vegetable Oil
EWf	Essential Work of Fracture
FESEM	Field Emission Scanning Electron Microscopy
FTIR	Fourier Transform Infrared Spectroscopy
IPN	Interpenetrating Polymer Network
ISO	International Organization for Standardization
LEFM	Linear Elastic Fracture Mechanics
MHHPA	Methylhexahydrophthalic Anhydride
OMMT	Organo-montmorillonite
PCR	Polymerase Chain Reaction
rDNA	Ribosomal Deoxyribonucleic Acid
SENT	Single Edge Notched Tensile
TEAB	Tetraethylammonium Bromide
TEM	Transmission Electron Microscopy
TGA	Thermogravimetry Analysis
XRD	X-ray Diffraction

## LIST OF SYMBOLS

$A$	Ratio of Absorbance
$a$	Initial Notched Length
$a/W$ Ratio	Notched Length-to-Width Ratio
$B$	Thickness of Specimen
$C$	Parameter of Diffusion Control
$^{\circ}\text{C}$	Degree Celcius
$C.I.$	Carbonyl Index
$D$	Diffusion Coefficient
$d$	Interlayer Spacing
$E$	Modulus of Elasticity
$E_a$	Activation Energy
$E'$	Storage Modulus
$F_{max}$	Maximum Load Applied
$h$	Sample Thickness
$\Delta H$	Change in Enthalpy
Hz	Hertz
J	Joule
$k$	Kinetic Rate Constant
$K_{IC}$	Fracture Toughness
$L$	Ligament Length
$m$	Kinetic Reaction Order
$M_m$	Maximum water uptake
$M_t$	Weight Gained at Any Time t
N	Newton
$n$	Kinetic Reaction Order
$\rho$	Density
Pa	Pascal
$R$	Gas Constant
$T$	Absolute Temperature
$T_5$	Temperature at 5% Weight Loss
$T_{10}$	Temperature at 10% Weight Loss

$T_d$	The Maximum Decomposition Temperature
$T_g$	Glass Transition Temperature
$T_{onset}$	Onset Curing Temperature
$T_{peak}$	Peak Temperature
$T_{max}$	The Maximum Degradation Rate
$t$	Time
$\tan \delta$	Damping Properties
$\nu_c$	Crosslink Density
$W$	Width of Specimen
$W_d$	Dry Weight of Specimen
$W_e$	Essential Work of Fracture
$W_p$	Non-Essential Work of Fracture
$w_e$	Specific Essential Work of Fracture
$\alpha$	Degree of Conversion
$\beta$	Shape Factor of Plastic Zone
$\beta w_p$	Specific Plastic Fracture Work
$\lambda$	Wavelength

# **PENYEDIAAN DAN PENCIRIAN TERMOSET, ADUNAN DAN NANOKOMPOSIT BERASASKAN MINYAK SOYA TEREPOKSIDA**

## **ABSTRAK**

Minyak soya terepokside (ESO) dimatangkan secara terma dengan menggunakan agen pematangan metilheksahidroftalik anhidrida (MHHPA) dan dua jenis pemangkin, iaitu 2-etil-4-metilimidazola (EMI) dan tetraetilamonium bromida (TEAB). Kinetik pematangan ESO/MHHPA telah dikaji menggunakan Spektroskopi Inframerah Jelmaan Fourier. Suhu pematangan dan kandungan pemangkin menunjukkan kesan-kesan yang ketara terhadap pemalar kadar, tindak balas tertib keseluruhan dan tenaga pengaktifan bagi sistem ESO/MHHPA. Penukaran kritikal didapati dalam lingkungan 0.6–0.8. Kinetik pematangan ESO/MHHPA dapat dihuraikan dengan lebih jelas dengan menambahkan faktor resapan di dalam model Kamal. Sifat-sifat terma termoset ESO telah dikajikan dengan penganalisa mekanik dinamik, penganalisa termogravimetrik, kalorimeter pengimbasan pembezaan dan pengukuran kandungan gel. Suhu peralihan kaca ( $T_g$ ), modulus storan, kandungan gel, ketumpatan sambung-silang, darjah penukaran dan kestabilan terma meningkat dengan penambahan kandungan EMI dan TEAB. Keliatan rekahan termoset ESO telah dikajikan dengan mekanik rekahan kenyal linear dan kerja terperlu untuk rekahan. Keliatan rekahan ( $K_{IC}$ ) dan kerja terperlu spesifik rekahan ( $w_e$ ) bagi termoset ESO meningkat dengan peningkatan kandungan EMI dan TEAB.  $K_{IC}$  dan  $w_e$  bagi termoset ESO akan berkurangan jika kandungan TEAB melebihi 0.5 phr. Keliatan rekahan, kerja terperlu spesifik rekahan dan kerja rekahan plastik spesifik bagi termoset ESO adalah dipengaruhi oleh jenis dan kandungan pemangkin. Ujian penyerapan air untuk termoset ESO telah dijalankan pada suhu bilik selama 3 bulan. Penyerapan air maksimum dan pekali peresapan termoset ESO berkurangan dengan peningkatan kandungan pemangkin. Dua strategi telah digunakan untuk

meningkatkan sifat-sifat mekanikal dan terma ESO, iaitu pengadunan ESO dengan diglisidil eter bisfenol-A (DGEBA) dan penguatan ESO dengan organo-montmorillonit (OMMT). Satu adunan yang terlarutcampurkan dengan struktur jaringan polimer saling menyusuk (IPN) telah dihasilkan dengan penambahan DGEBA ke dalam ESO. Struktur IPN boleh dibuktikan dengan mikroskopi elektron pemancaran dan mikroskopi daya atomik. Peningkatan sinergi dalam modulus, kekuatan tegangan,  $T_g$ , ketumpatan sambung silang dan kestabilan terma bagi adunan ESO/DGEBA boleh dikaitkan dengan jaringan saling menyusuk dalam adunan. Sifat-sifat mekanikal dan terma ESO juga dapat ditambah baik dengan penambahan OMMT. Peningkatan sifat-sifat sedemikian adalah disebabkan oleh kesan ko-mangkin daripada oktadesil trimetil amonium (interlarut OMMT) yang memudahkan pematangan terma ESO dan mempromosikan pembentukan sambung silang. Penguraian ESO dalam tanah kompos juga dikaji. Termoset ESO dapat diuraikan oleh mikroba tanah dalam persekitaran tanah kompos. Takat biodegradasi bagi ESO telah ditentukan daripada penyukat perubahan berat. Kehilangan berat bagi ESO adalah dipengaruhi oleh ketumpatan sambung-silang dan masa pendedahan penanaman dalam tanah. Merujuk kepada keputusan pendekatan jajaran 16S rDNA, *Comamonas* sp., *Bacillus* sp., *Streptomyces* sp. dan *Acinetobacter* sp. merupakan mikroba tanah yang berkemungkinan besar boleh menguraikan ESO.

# PREPARATION AND CHARACTERIZATION OF EPOXIDIZED SOYBEAN OIL BASED THERMOSET, BLENDS AND NANOCOMPOSITES

## ABSTRACT

Epoxidized soybean oil (ESO) was thermally-cured with methylhexahydrophthalic anhydride (MHHPA) curing agent in the presence of two different types of catalysts, i.e., 2-ethyl-4-methylimidazole (EMI) and tetraethylammonium bromide (TEAB). The cure kinetics of ESO/MHHPA was studied using the Fourier Transform Infrared Spectroscopy. The cure temperatures and catalyst contents showed significant effects on the kinetic rate constants, overall reaction orders and activation energies of ESO/MHHPA systems. The critical conversion was found to be 0.6–0.8. Cure kinetics of ESO could be well-described by adding the diffusion factor into Kamal's model. The thermal properties of ESO thermosets were studied by dynamic mechanical analyzer, thermogravimetry analyser, differential scanning calorimetry and gel content measurement. The glass transition temperature ( $T_g$ ), storage modulus ( $E'$ ), gel content, crosslink density, degree of conversion and thermal stability increased with increasing EMI and TEAB content. The fracture toughness of ESO thermosets was studied using linear elastic fracture mechanics and essential work of fracture. The fracture toughness ( $K_{IC}$ ) and the specific essential work of fracture ( $w_e$ ) of the ESO thermosets increased with increasing the EMI and TEAB content. A reduction in  $K_{IC}$  and  $w_e$  of the ESO thermosets were found if the TEAB content exceeded 0.5 phr. The water absorption test for ESO thermosets was conducted at room temperature for 3 months. The maximum water uptake and the diffusion coefficient of the ESO decreased with increasing catalyst content. Two strategies, i.e., blending with the diglycidyl ether of bisphenol-A (DGEBA) and reinforcing with organo-montmorillonite clay (OMMT), were used to improve the mechanical and thermal properties of ESO. A miscible blend with an interpenetrating polymer network (IPN)

structure was obtained by adding DGEBA into ESO. The IPN structure was evidenced by transmission electron microscopy and atomic force microscopy. The synergistic enhancement in modulus, tensile strength,  $T_g$ , crosslink density and thermal stability of the ESO/DGEBA blends could be associated to the possible interpenetrating network of the blends. These mechanical and thermal properties of ESO were also improved by the addition of OMMT. Such improvements arose from the co-catalytic effect of octadecyl trimethyl ammonium (intercalant of OMMT) to facilitate the cure reaction of ESO, that in turn promoted the crosslink formation. The biodegradability of ESO in the compost soil was also studied. ESO thermosets were biodegraded by the soil microbes under the compost soil environments. The extent of biodegradation of ESO was determined from weight change measurement. It was found that the weight loss of ESO was governed by the crosslink density and soil-buried exposure time. From the 16S rDNA sequencing approach, it was determined that *Comamonas* sp., *Bacillus* sp., *Streptomyces* sp. and *Acinetobacter* sp. are the possible soil microbes to degrade the ESO.

# CHAPTER 1

## INTRODUCTION

### 1.1 Research Background

Polymers produced from sustainable and renewable natural resources have received considerable attention today. Natural oils derived from plant resources are important renewable raw materials used in polymer industry. It is forecasted that vegetable oils will play a key role during the 21<sup>st</sup> century as one of the most promising resources for bio-based polymers (Seniha Guner et al., 2006). Recently, soybean oils have been functionalized by using several approaches, for example, epoxidation, metathesis of unsaturated fatty acids, acrylation of epoxies, reaction with the maleic anhydride and transesterification (Ortiz et al., 2005; Lin et al., 2008). Epoxidation of soybean oils is one of the most important reactions in organic synthesis to transform the soybean oils into polymerizable epoxidized soybean oil (ESO) monomers among those reactions.

Conventionally, ESO are widely used as poly(vinyl chloride) additives and as a starting material to produce the polyol and polyurethane foam (Rosli et al., 2003; Lin et al., 2008). In recent years, ESO have been utilized as starting materials to prepare thermosetting materials attributed to their renewability, availability, high reactivity of oxirane rings and versatility. In this respect, bio-based thermosetting materials can be produced by curing the ESO through thermal and UV approaches (Crivello & Carlson, 1996; Gerbase et al., 2002).

The curing mechanisms of ESO resins have been studied and documented in the literature. Gao (2008) proposed that the curing mechanisms of the catalytic ESO-anhydride thermosets involves the reaction of tertiary amine with the ESO monomer, followed by the ring opening of the anhydride functional groups with the alkoxide.

Ortiz et al. (2005) reported that the radical polymerization of ESO thermoset in the presence of diaryliodonium salt photo-initiator follows both conventional cationic polymerization and chain reaction mechanisms. Jin & Park (2007) proposed thermal-induced ring opening polymerization route for the ESO thermoset initiated by the *N*-benzylquinoxalinium hexafluoroantimonate thermal latent initiator.

Researchers have also studied and modelled the cure kinetics of vegetable oil-based resins, particularly the epoxidized triglyceride oils, to control and optimize the curing schedules and processing conditions in preparing the thermosetting materials. Boquillon & Fringant (2000) modelled the cure kinetics of the epoxidized linseed oil/tetrahydrophthalic anhydride (ELO/THPA) system catalyzed with 2-methylimidazole (2MI). The curing reaction of 2MI-catalyzed ELO/ THPA system was found to obey the first-order kinetic law. Liang & Chandrahekhara (2006) used Kamal's equation to model the cure kinetic of soy-based epoxy resin. The overall reaction order of the soy-based epoxy resin system was determined to be approximately two. Martini et al. (2009) studied the cure kinetics of epoxidized linseed oil methyl esters with different cyclic dicarboxylic anhydrides. Manthey et al. (2011) modelled the curing behaviour of an epoxidized hemp oil based bioresin system using dynamic and isothermal cure kinetics. Mahendran et al. (2012) used the free kinetic method to model the cure kinetics of epoxidized linseed oil in the presence of methyl nadic anhydride (as a curing agent) and 1-methylimidazole (as a catalyst).

Even if several approaches can be used to prepare ESO-based thermosetting materials, they tend to suffer from the shortcomings in terms of poor thermo-physical properties. In this respect, some strategies have been implemented to improve the mechanical and thermal properties of ESO thermoset, for example, addition of fibers (Takahashi et al., 2008; Shibata et al., 2009; Shibata et al., 2011; Retegi et al., 2012),

incorporation of clay (Uyama et al., 2003; Liu et al., 2005; Tanrattanakul & Saithai, 2009), hybridization with maleated soybean oil and maleated methyl soyate (Tran et al., 2006), modification with silane coupling agent (Tsujimoto et al., 2010), and blending with petroleum-based epoxy (Ratna, 2001; Jin & Park, 2008a; Gupta et al., 2011; Altuna et al., 2011).

A few studies have also focused on the biodegradation of ESO thermosets in the last few years. Accordingly, ESO was found to be readily biodegradable when being landfilled in soil (Kurata et al., 2009). This is due to the fact that the fatty acid residues in ESO could be easily attacked by the lipase secreting bacteria and being mineralized into the water and carbon dioxide (Xu et al., 2002). However, the biodegradability of ESO thermosets is majorly affected by the crosslink density, type of crosslink linkages and the nature of curing agents. It has been reported that the highly-crosslinked ESO thermosets with non-degradable ether linkages and with the amine type linkages were hardly to be mineralized and biodegraded, while the ESO thermosets crosslinked with the hydrolysable ester linkages were more readily to be cleaved by esterase and biodegraded by microbial enzymes in soil (Shogren, 1999; Shogren et al., 2004).

## **1.2 Problem Statement**

Polymers from vegetable oils derivatives such as ESO offer many unique advantages and new beneficial properties. However, a long curing schedule and high temperature of curing were required to prepare ESO thermosets. Gerbase et al. (2002) stated that ESO can be thermal-cured with various cyclic acid anhydrides (i.e., succinic, phthalic, hexahydrophthalic and maleic anhydrides) in the presence of triethylamine catalyst at 150°C for 14 h. Jin & Park (2007) reported that the thermal curing conditions of the

ESO/*N*-benzylquinoxalinium hexafluoroantimonate systems are 110°C for 1 h, then 140°C for 2 h and finally at 170°C for 2 h. Espana et al. (2012) found that ESO resin can be thermal-cured with maleic anhydride in the presence of dimethylbenzylamine accelerator and 1,3-butanediol initiator by following the thermal curing cycle: 100°C for 1.5 h, 120°C for 2 h and 160°C for 1 h.

Moreover, ESO thermosets have limitations in terms of poor mechanical and thermal properties. It has been documented that the glass transition temperature ( $T_g$ ) and storage modulus ( $E'$ ) of ESO thermosets were in the range of 24–65°C and 8–16 MPa, respectively (Gerbase et al., 2002; Park et al., 2004; Jin & Park, 2007; Gupta et al., 2010; Espana et al., 2012). Also, it was reported that the tensile strength and the Young's modulus of ESO thermoset thermal-cured using triethylenetetramine curing agent were 1.27 MPa and 1.20 MPa, respectively (Liu et al., 2005). Pan et al. (2011) determined that ESO cured with 4-methyl-1,2-cyclohexanedicarboxylic anhydride in the presence of 1,8-diazabicyclo[5.4.0]undec-7-ene amine catalyst possessed tensile strength and tensile modulus of about 10.2 MPa and 65 MPa, respectively. Shibata et al. (2011) found that the tensile strength and modulus of ESO cured with tannic acid were 4.4 MPa and 54 MPa, respectively. The mechanical and thermal properties are rather inferior and serve as the limiting factor for some of the advanced applications of ESO thermosets where high rigidity, strength, and  $T_g$  are required.

It has been reported that ESO thermosets may biodegrade under the natural environment. However, there has been very limited research work published on the biodegradability of ESO thermosets. Moreover, few reports have only mentioned that ESO thermosets could be mineralized by soil microorganisms, but there is no work done in order to isolate and identify the bacterial colonies which have the potential to mineralize and biodegrade the ESO thermosets.

### **1.3 Hypothesis and Motivation**

The cure kinetic study was performed in this study to understand the reaction process of ESO through the utilising of two types of catalysts, i.e., 2-ethyl-4-methylimidazole and tetraethylammonium bromide. It is hypothesized that the processing conditions of ESO (i.e., cure temperature and cure time) can be optimized by performing the cure kinetics study. In this respect, the ESO thermosets can be prepared by using a shorter cure schedule (i.e., 3 h) and lower cure temperature (i.e., 140°C) in the presence of EMI or TEAB catalyst. It is also believed that the mechanical and thermal properties of the ESO thermosets can be enhanced by using two strategies, i.e., blending with the bifunctional epoxy (diglycidyl ether of bisphenol-A, DGEBA) and reinforcing with organo-montmorillonite clay (OMMT). Furthermore, the possible soil microbes and bacterial colonies that may involve in the biodegradation of ESO thermosets can be isolated and identified.

### **1.4 Research Objectives**

The objectives of the present work are:

1. To investigate the cure kinetics and develop the cure kinetic models for ESO thermosetting materials.
2. To examine the effect of 2-ethyl-4-methylimidazole and tetraethylammonium bromide catalysts on the cure characteristics, fracture behaviours, thermal and physical properties as well as kinetics of water absorption for ESO thermoset.
3. To improve the mechanical and thermal properties of the ESO thermosets by means of blending with a bi-functional epoxy and reinforcing with the organoclay.

4. To study the biodegradability of ESO thermosets in the natural soil burial environment and identify the possible bacteria colonies that can biodegrade the ESO thermoset.

### **1.5 Research Scopes**

The research scopes of the study covered 4 main phases. The 1<sup>st</sup>-phase was to study the fundamental aspects of cure kinetics of ESO thermosets using Fourier Transform Infrared Spectroscopy (FTIR) method. The 2<sup>nd</sup>-phase involved the preparation of the ESO thermoset, in which the ESO resin was cured with the methylhexahydrophthalic anhydride (MHHPA) curing agent in the presence of two types of catalysts, i.e., 2-ethyl-4-methylimidazole (EMI) and tetraethylammonium bromide (TEAB), of various loadings. The mechanical, thermal and physical properties, as well as the cure characteristics and the kinetics of water absorption for the ESO thermosets were characterized by means of various analytical methods. The 3<sup>rd</sup>-phase encompassed the reinforcement of ESO by the OMMT and by blending the ESO with DGEBA, followed by characterizing ESO/DGEBA blends and ESO/OMMT nanocomposites. The 4<sup>th</sup>-phase was to evaluate the bio-degradability of ESO thermosets in the natural soil environment and to identify the bacterial colonies, which could possibly degrade the ESO thermosets.

### **1.6 Structure of Thesis**

This thesis basically consists of five chapters.

Chapter 1 provides the overview of the research and a brief literature survey of the previous works. The problem statement, the hypothesis and motivation, the research

objectives and the scopes of research for the present study have also been stated and described in this chapter.

Chapter 2 highlights the detailed literature survey and intensive review of previous research works and recent progress in developing, preparing and characterizing ESO based thermosets, blends and nanocomposites.

Chapter 3 presents the raw materials, methods and equipments used in the present work. The preparation procedures of ESO based thermoset, blends and nanocomposites have also been described in details.

Chapter 4 gives the interpretation and discussion of the experimental results of the research work. The cure kinetics, soil-burial biodegradability and the properties of ESO based thermosets, blends and nanocomposites (i.e., mechanical, thermal, physical, morphology and water absorption) have been discussed intensively in this chapter.

Chapter 5 presents the significant results and summary of the research study. The recommendations for the future studies in the related research are included in this chapter.

## CHAPTER 2

### LITERATURE REVIEW

#### 2.1 Vegetable Oils

Vegetable oils with the molecular structure as shown in Figure 2.1 have attracted the attention worldwide in recent years. The interest can be justified by the versatility of vegetable oil constituents which are made up of complex multi-components mixtures of fatty acids and glycerol esters.

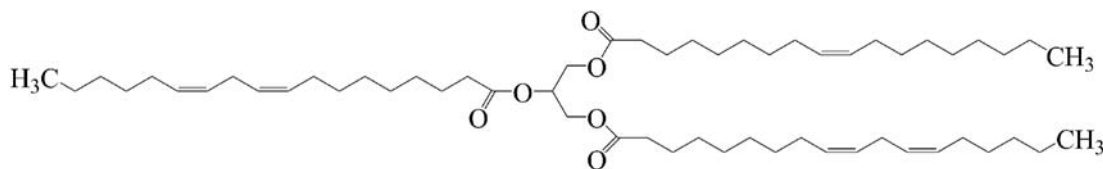


Figure 2.1: Typical chemical structure of vegetable oils (Girma & Kashmiri, 2008)

In general, advances in oleo-chemistry technology today makes possible for researchers to chemically modify and transform the vegetable oils into polymerizable monomers via epoxidation, reaction with maleic anhydride, metathesis of unsaturated double bonds, acrylation of epoxies and transesterification (Ortiz et al., 2005; Lin et al., 2008). Among those reactions, epoxidation is a commercially important reaction in organic synthesis since the high reactivity of epoxy rings makes them to be readily transformed into desired functionality (Gerbase et al., 2002; Goud et al., 2006; Dinda et al., 2008). As a result, many researches on the epoxidation of vegetable oils have been conducted in order to optimize the conversion rate of epoxidation and increase the epoxy yield.

Phileshajev-epoxidation, chemo-enzymatic epoxidation, catalytic epoxidation with acidic ion exchanged resin and metal-catalyzed epoxidation are 4 main methods commonly used to transform the vegetable oils into useful polymerizable oxygenated monomers. Different epoxidation processes for various types of vegetable oils, their efficiency, selectivity and epoxy content are summarized in Table 2.1. Among those methods, the chemo-enzymatic epoxidation has received considerable interest in late as the method is safe, environmental friendly and the conversion rate of epoxidation usually exceeds 90.0% (Klass & Warwel, 1999). Typically, those vegetable oils with high content of unsaturated fatty acids especially soybean and linseed oils (ref. Table 2.2) are only chosen to be epoxidized in order to reaffirm a higher conversion of the double bonds from fatty acid into epoxy functions.

### **2.1.1 Types of Vegetable Oils**

There are plenty of vegetable oils such as canola oil, corn oil, olive oil, cottonseed oil, linseed oil, palm oil, rapeseed oil, soybean oil, etc. available worldwide at the present time (Khot et al., 2001). According to the statistics of the world vegetable oil consumption as illustrated in Figure 2.2, it was found that the global vegetable oils consumption grew linearly year over year. This growing trend was believed to be attributed to the versatility of the vegetable oil constituents which made possible for researchers to make full use of vegetable oils (Lin et al., 2008; Ortiz et al., 2005).

Accordingly, it was determined that palm oil, soybean oil, sunflower oil and linseed oil were the 4 most important vegetable oils worldwide, holding a share of more than 80% of the market (Yusof & Yew, 2009). It was also forecasted that the consumption of these 4 types of oils will increase about 18.3% by 2015 compared with the year of 2009 due to the rapid population growth and the improvement in the living standards of the population wide sections (Frank et al., 2009).

Table 2.1: Different epoxidation process of various types of vegetable oils, and their efficiency, selectivity and epoxy content

Epoxidation Process	Vegetable Oil	Processing Conditions		Efficiency (%)	Selectivity (%)	Epoxy Content (%)	References
		$T$ (°C)	$t$ (h)				
Conventional	Jatropha	50	10	87.4	-	4.8	Meyer et al. (2008)
	Soybean	50	10	83.3	-	6.1	Meyer et al. (2008)
		75	4	-	-	6.3	Cai et al. (2008)
	Cottonseed	60	4	77.0	-	-	Dinda et al. (2008)
Acidic Ion Exchange Resin (AIER)	Canola	65	7	90.8	-	-	Mungroo et al. (2008)
	Soybean	75	8	91.5	87.0	6.0	Sinadinovic-Fiser et al. (2001)
		60	4	99.4	95.0	-	Petricic et al. (2002)
Chemo-Enzymatic	Rapeseed	RT	16	99.0	92.0	5.3	Klass & Warwel (1999)
	Linseed	RT	16	98.0	98.0	9.9	Klass & Warwel (1999)
	Soybean	50	24	98.9	-	6.9	Vlcek & Petrovic (2006)
		RT	16	99.0	94.0	7.1	Klass & Warwel (1999)
	Sunflower	30	16	> 99.0	-	-	Schneider et al. (2009)
Metal-Catalyzed		RT	16	88.0	100.0	6.3	Klass & Warwel (1999)
	Soybean	RT	2	95.0	95.0	-	Gerbase et al. (2002)
	Sunflower	60	6	99.0	-	7.6	Mohamed et al. (2007)
	Unsaturated fatty acid	30	2	96.0	95.0	-	Cai et al. (2009)

Table 2.2: List of fatty acid profiles in some vegetable oils (Meyer et al., 2008)

Fatty Acid	Vegetable Oils				
	Palm	Jatropha	Soybean	Sunflower	Flax Seed
Lauric (C12/0)	-	-	-	0.5	-
Myristic (C14/0)	-	-	0.1	0.2	-
Palmitic (C16/0)	40.3	14.2	11.0	4.8	5.0
Palmitoleic (C16/1)	-	1.4	0.1	0.8	-
Stearic (C18/0)	3.1	6.9	4.0	5.7	4.0
Oleic (C18/1)	43.4	43.1	23.4	20.6	19.0
Linoleic (C18/2)	13.2	34.4	53.2	66.2	14.0
Linolenic (C18/3)	-	-	7.8	0.8	58.0
Arachidic (C20/0)	-	-	0.3	0.4	-
Behenic (C22/0)	-	-	0.1	-	-
Saturates	43.4	21.1	15.5	11.6	9.0
Unsaturates	56.6	78.9	84.5	88.4	91.0

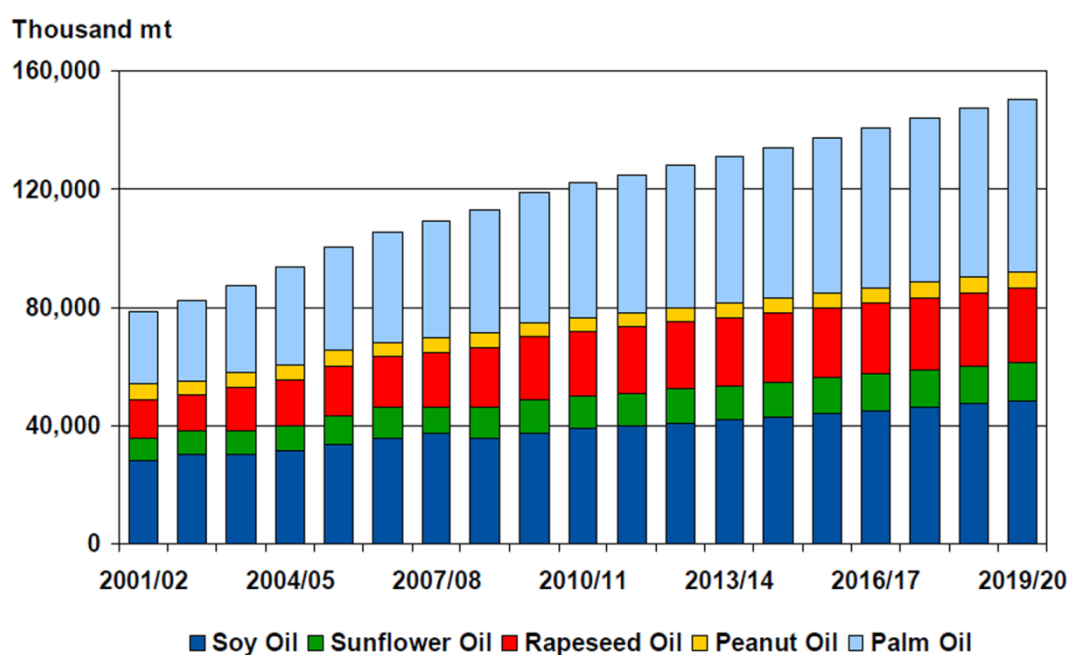


Figure 2.2: Global vegetable oil consumption (<http://www.fapri.com>)

Traditionally, soybean oil was the most popular vegetable oil used attributed to its availability and its price is not expensive. As an example, Clayton (1988) stated that 90% of the market was commercially monopolized by the soybean oil in 80s'

whereas Miyagawa et al. (2006) reported that 500 millions pounds out of 16 billion pounds of soybean oil produced by United States agricultural annually was utilized in industry application nowadays. Even if soybean oil was the leading vegetable oil in world consumption in the year of 2006, Van et al. (2006) reported that palm oil would come to the level with and pass the soybean oil within the next few years. As shown in Figure 2.2, palm oil has surpassed soybean oil as the world's most popular vegetable oil today.

### **2.1.2 Vegetable Oil Producers**

In the year of 2000, Yusof (2002) reported that Malaysia monopolized half of the world palm oil production. Palm oils were granted priority in Malaysia due to their superior sustainability and availability (Rosli et al., 2003). About 80 to 85% of the total world production of palm oil was dominated by Malaysia and Indonesia in 2008, in which, they were holding a world market share of approximately 31% (Frank et al., 2009). Besides Malaysia and Indonesia, other palm oil producing countries included South America, Sub-Saharan Africa, Thailand and Colombia (Yusof, 2002; Frank et al., 2009).

According to Cai et al. (2008), it was determined that the world production of soybean oil was almost 200, 000 tonnes/year. Being the second of the world's largest commodities after palm oil which held a world market share of 28% in the year of 2008, soybean oil was globally produced by USA, China, Argentina, Brazil, ES, and India (Yusof & Yew, 2009; Frank et al., 2009). Among these countries, USA was categorized as the largest producer of soybean oil since USA annually produced one billion pounds of soybean oil exceeding the current commercial demand (Xu et al., 2002).

### **2.1.3 Global Use of Vegetable Oils**

The global use of vegetable oils was basically classified into two main categories: (i) food industry, and (ii) industrial application (Frank et al., 2009). The largest proportion of vegetable oils, approximately 80%, was utilized for food, while the share was taken up by the industrial sectors. Among the industrial market share, animal feed, bio-fuels and oleochemicals took up the market share of 6%, 5% and 10%, respectively (Yusof & Yew, 2009).

Recently, market for vegetable oil-based materials for industrial applications were expanding rapidly as the result of the environmental issue, the depletion of non-renewable resources and waste disposal problem (Miyagawa et al., 2005; Meyer et al., 2008). Therefore, vegetable oils with the oxirane groups which were believed to be an ideal alternative to the petrochemical-based feedstock were accepted as an important oleochemicals lately (Klass & Warwel, 1999; Cai et al., 2009). These vegetable oils were commonly used as poly(vinyl chloride) plasticizers, stabilizers, lubricants and starting materials to produce polyols, pre-polymers in surface coating formulations and to synthesize of polyurethane foams (Rosli et al., 2003; Lin et al., 2008). Also, modified vegetable oils could be used to improve the efficiency of the fabrication process of linoleum floor cloth, to modify other thermoset polymers and to synthesize new polymers that were appropriate for liquid moulding (Hilker et al., 2001; Xu et al., 2002; Miyagawa et al., 2005).

## **2.2 Epoxidized Soybean Oil**

Soybean oil as illustrated in Figure 2.3 is an unsaturated triglyceride, which consists primarily of the stearic, oleic, linoleic and linolenic fatty acids (Parreira et al., 2002; Salih et al., 2011). The unsaturated free fatty acids in soybean oil (i.e., oleic, linoleic and linolenic acids) have been commercially functionalized by introducing the epoxy

groups to transform the soybean oil into polymerizable epoxidized soybean oil (ESO) monomer (Adhvaryu & Erhan, 2002; Seniha Guner et al., 2006; Holser, 2008). In general, the unsaturated double bonds in vegetable oils can be epoxidized into a three membered epoxy ring with various peracids. Accordingly, the mechanisms of ESO preparation involve 2 stages: (i) an *in-situ* reaction of the formation of peracids (i.e., peracetic acid or performic acid) from hydrogen peroxide and carboxylic acid in the presence of a strong mineral acid, and (ii) the epoxidation of unsaturated fatty acids with peracids (Cai et al., 2008; Meyer et al., 2008).

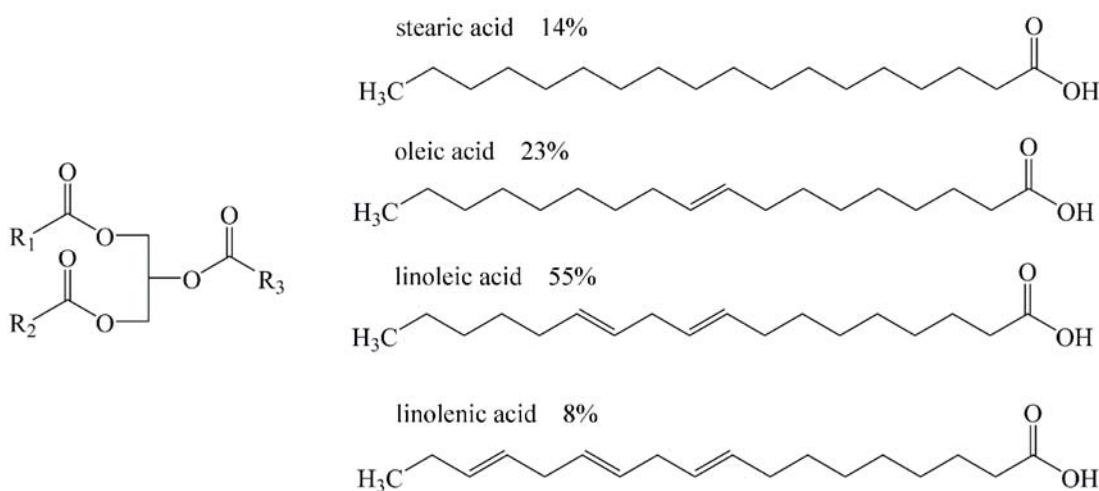


Figure 2.3: Structure of soybean oil and its substituted fatty acids (Parreira et al., 2002)

The functionalized oleic, linoleic and linolenic fatty acids in ESO resin could be cured via the thermal and UV approaches to form a crosslinked thermoset with 3-dimensional network structure (Crivello & Carlson, 1996; Gerbase et al., 2002; Ortiz et al., 2005; Jin & Park, 2007; Gupta et al., 2010; Kim & Sharma, 2012). However, saturated fatty acids in ESO resin (i.e., palmitic and stearic acids) do not take part in the polymer network formation. This is attributed to the fact that they do not possess any epoxy functional groups in their backbone structure.

## 2.2.1 Curing Reaction of Epoxidized Soybean Oil

Rocks et al. (2004) reported on the thermal curing mechanisms of ESO with *t*-amines and anhydrides. The proposed curing mechanism for catalytic ESO-anhydride system is shown in Figure 2.4. It has been reported that the *t*-amine would first react with the ESO monomer to form the zwitterions during the initiation reaction (Reaction 2.1). The alkoxide from the zwitterions would then chemically react with the anhydride to yield carboxylate anions (Reaction 2.2). Propagation reaction involved the reaction of the carboxylate anions with the oxirane group in ESO producing the new alkoxide (Reaction 2.3). The alkoxide formed then reacted with another anhydride in order to regenerate the carboxylate anions (Reaction 2.4) and propagate the curing cycle.

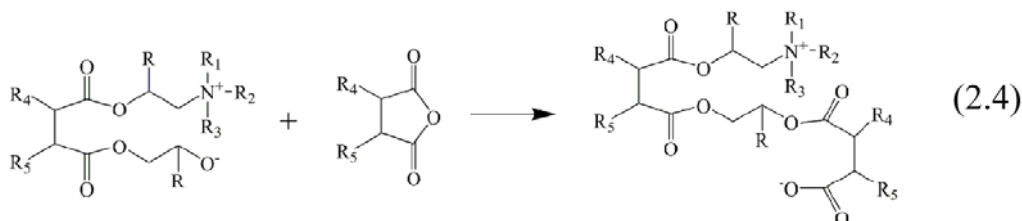
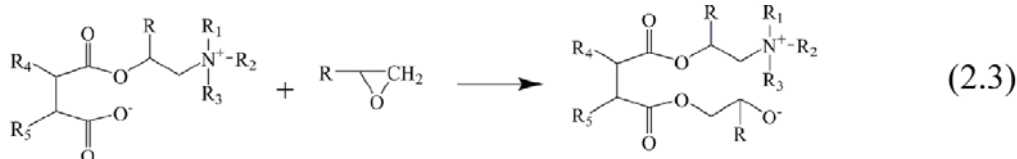
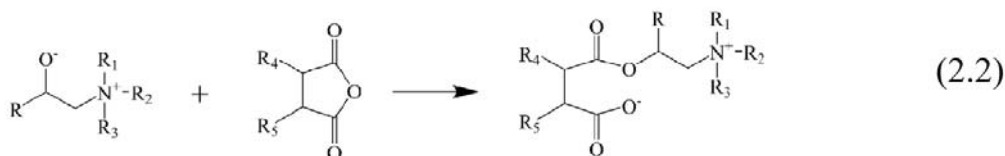
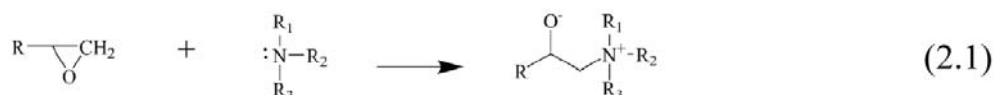


Figure 2.4: Cure mechanism of ESO resin with *t*-amines and anhydrides (Rocks et al., 2004)

Ortiz et al. (2005) reported the radical-induced cationic photo-polymerization of the ESO in the presence of onium salt cationic photoinitiators. The cationic photo-polymerization mechanism of the ESO systems is shown in Figure 2.5. Referring to Figure 2.5, a protonic acid that could initiate the polymerization was generated from the diaryliodonium salt through the conventional cationic polymerization mechanism (Reaction 2.5). The anions of the diaryliodonium salt (protonic acid) would then react with the ESO resin to initiate the polymerization reaction (Reactions 2.6 – 2.7). The radicals derived from the photolysis of photo-initiator abstracted the labile hydrogen atom of the ESO monomers to yield the monomer-bound cation by the chain reaction mechanisms (Reactions 2.8–2.10). These  $R^+M_tX_n^-$  cations generated from the chain reaction could initiate the photo-polymerization of ESO monomers yielding ESO thermoset with 3-dimensional crosslinked network structure.

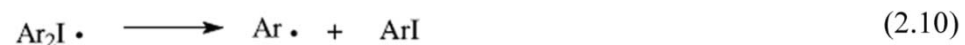
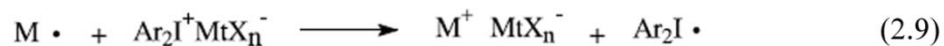
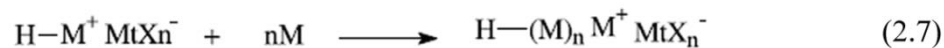
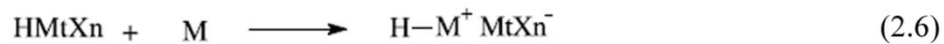
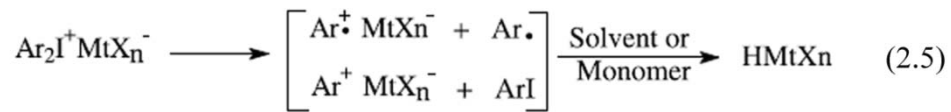


Figure 2.5: Schematic represents the cationic photopolymerization mechanism of ESO in the presence of onium salt cationic photoinitiator (Ortiz et al., 2005)

Jin & Park (2007) studied the thermal-induced ring opening polymerization of internal oxirane rings in ESO initiated by the *N*-benzylquinoxalinium hexafluoroantimonate (BQH). Figure 2.6 shows the proposed thermal curing mechanisms of the ESO resin in the presence of BQH thermal latent initiator.

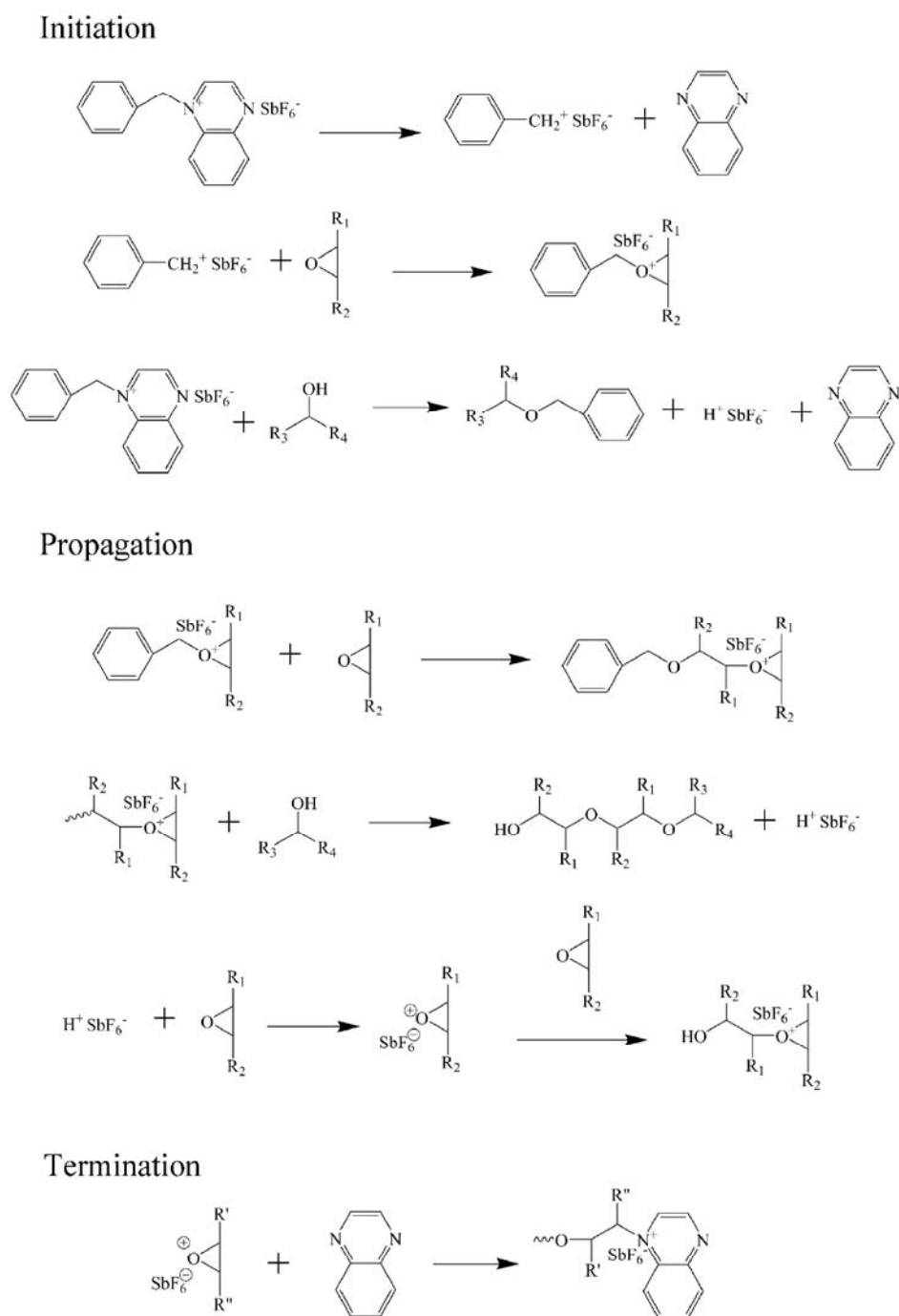


Figure 2.6: Thermal induced ring-opening cationic polymerization of internal epoxies in ESO initiated by BQH thermal latent initiator (Jin & Park, 2007)

Referring to Figure 2.6, a benzyl cationic initiating species was formed from the thermally-decomposed BQH during the initial polymerization stage. The oxirane groups in the ESO would then react with the propagating cationic species during the initial propagating stage. Propagation reaction would proceed through a subsequently attack of epoxy groups in ESO. This promoted the esterification of ESO. The curing reactions stop once the concentration of monomer species decreased dramatically. Espana et al. (2012) proposed the thermal curing mechanisms for the benzyl-dimethylamine catalyzed ESO/maleic anhydride systems. The reaction mechanism is shown in Figure 2.7. The initiation reaction involved the ring opening of the maleic anhydride by the hydroxyl groups to produce a monoester with the carboxylate group (Reaction 2.11). The monoester formed would react with the oxirane groups in the ESO to yield a diester and a new secondary hydroxyl group (Reaction 2.12). The intermediate species generated would then ring open other anhydrides and oxirane groups of ESO to propagate the curing cycles (Reaction 2.13).

In short, ESO resin can be cured by thermal and UV. The curing mechanisms of ESO basically involve 3 distinct stages, i.e., initiation, propagation and termination. Accordingly, the cure reaction of ESO involves either (i) the attack of electrophiles on the oxygen atom or (ii) the nucleophile attack on one of the two carbon atoms on the oxirane ring of ESO. Nevertheless, both initiation mechanisms generate the reaction intermediates which can propagate the curing cycles. Hence, it can be concluded that the curing mechanisms of ESO resin is governed by the curing techniques (e.g., thermal or ultraviolet) and types of reagents (e.g., catalyst, curing agent, and photo-initiator) used in the curing of ESO.

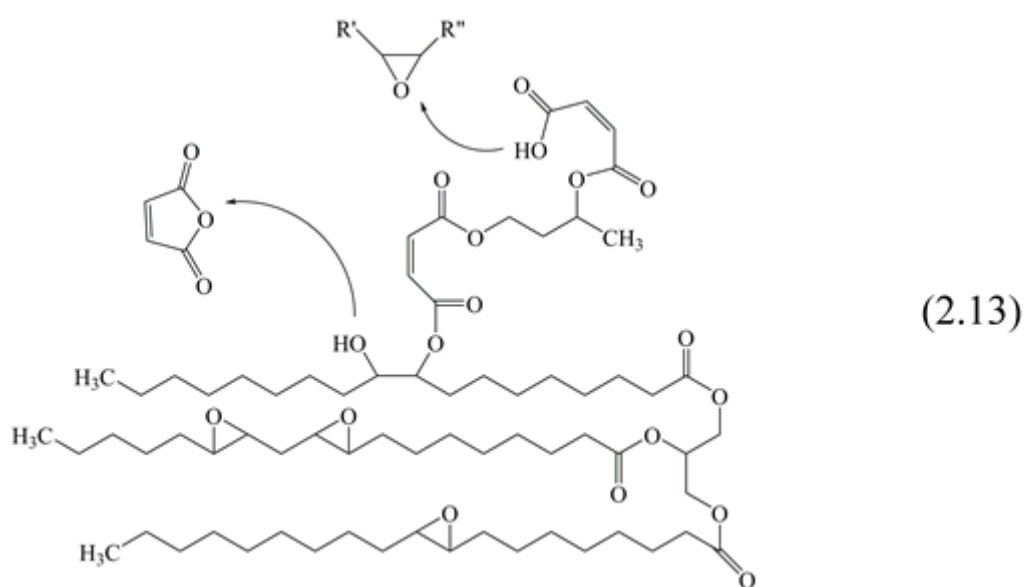
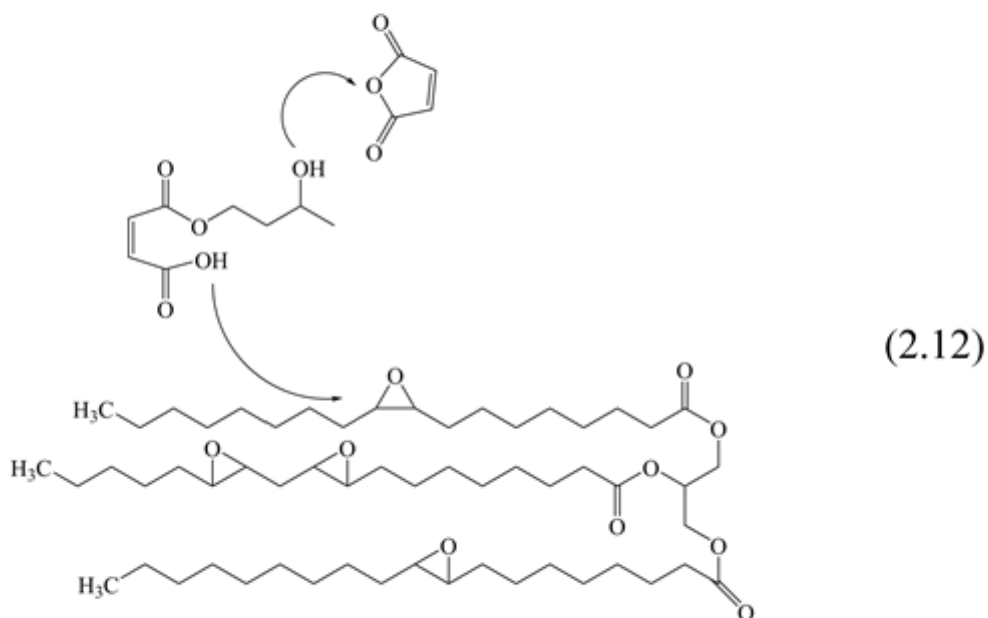
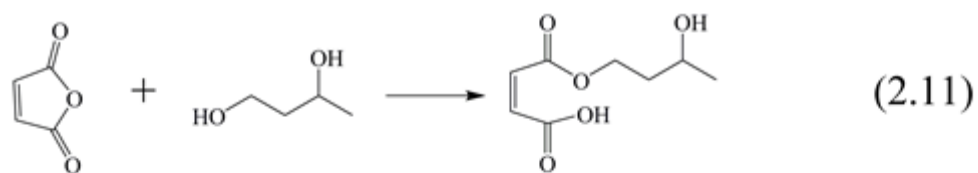


Figure 2.7: Schematic curing mechanism of ESO/maleic anhydride reaction (Espana et al., 2012)

### 2.2.2 Properties of Epoxidized Soybean Oil Thermoset

Gerbase et al. (2002) investigated the mechanical and thermal behaviours of the ESO resin cured with various cyclic anhydrides, in the presence of tertiary amine initiator. The dynamic mechanical analysis (DMA) results showed that ESO thermosets cured with anhydrides with rigid structures such as phthalic, maleic, and hexahydrophthalic exhibited high glass transition temperature ( $T_g$ ) and crosslink density ( $\nu_c$ ). It was also found that both the PA- and MA-cured systems showed higher dynamic mechanical properties (i.e., storage modulus) than that of those succinic and dodecenylsuccinic anhydride cured ESO thermosets.

Park et al. (2004) reported the thermal properties of the ESO and epoxidized castor oil (ECO) resins initiated by *N*-benzylpyranium hexafluoroantimonate (BPH) cationic initiator. The cationic polymerization reactions of both ESO and ECO could only be initiated by BPH at 80°C and 50°C, respectively. The DMA results indicated that the crosslink density and storage modulus of ESO thermosets were higher than that of the ECO thermosets attributed to the higher content of reactive epoxy groups in ESO. The thermomechanical analysis results implied that the ECO/BPH thermoset showed a higher  $T_g$  value and lower coefficient of thermal expansion than those of ESO, due to the higher intermolecular interaction in the ECO/BPH system.

Xu et al. (2004) studied the viscoelastic properties of polymerized ESO with two types of curing agents (i.e., triethylene glycol diamine and triethylenetriamine). It was determined that type and amount of crosslinking agents used would affect the glass transition temperature ( $T_g$ ) and viscoelastic behaviours of ESO thermosets. The ESO crosslinked by the short-armed triethylenetriamine crosslinking agent showed a higher  $T_g$  and complex modulus ( $G^*$ ) than those cured by the long-armed triethylene

glycol diamine. Furthermore, it was also noteworthy to mention that the viscoelastic properties of ESO thermosets were similar to some synthetic rubbers or plastics.

Ortiz et al. (2005) conducted a kinetic study of the accelerated effect of the mono-, di- and tri-substituted alcohols on cationic polymerization rate of ESO. It was initially determined that the rate of conversion of ESO resin was low. As a result, the polymerization rate of ESO was accelerated using alcohols. The addition of 20% of the 2,5-dimethoxybenzyl alcohols could maximize the photopolymerization rate of the ESO system.

Jin & Park (2007) studied on the thermal properties of ESO- and epoxidized castor oil (ECO) thermosets. Experimental evidence from dynamic differential scanning calorimetry (DSC) thermogram showed that the cure activation energy and the peak maximum temperature and of ESO thermosets were higher than the ECO thermosets. This is due to the steric hindrance induced by intermolecular interactions between the ESO and *N*-benzylquinoxalinium hexafluoroantimonate (BQH) initiator. Thermogravimetric analysis (TGA) thermograms showed that the temperature at the maximum degradation rate ( $T_{max}$ ) and the initial decomposition temperature of ESO thermosets were greater than the ECO thermosets, which is attributed to the higher crosslink density of ESO/BQH system.

Gupta et al. (2010) determined that the epoxy/anhydride ratios can affect the dynamic mechanical properties, glass transition temperatures, impact strength and thermal stability of the ESO thermoset. These properties would be increased with an increase in the hardener content up to a stoichiometric equivalent after which there was a drop. However, the peak factor values (full width at half maximum of the  $\tan \delta$  peak divided by its height) of ESO thermosets increased with increasing the ratio of epoxy/anhydride even if passing through a maximum at the stoichiometric ratio.

Espana et al. (2012) studied the mechanical, thermal and thermo-mechanical properties of ESO under the influence of the equivalent epoxide weight to anhydride equivalent weight ratio (EEW:AEW ratio) between ESO resin and maleic anhydride. It was found that the EEW:AEW ratio of 1:1 was the optimum stoichiometric ratio to produce ESO thermoset with a balance of flexural, hardness and impact properties. Also, the optimum thermal properties (i.e., glass transition temperature, coefficient of thermal expansion, heat deflection temperature and the Vicat softening temperature) could be obtained for ESO thermosets with an EEW:AEW ratio of 1:1. It was also expected that ESO thermosets with the maximum crosslink density could be prepared using this stoichiometric ratio.

Based on these research findings, it can be summarized that the mechanical and thermal properties of ESO thermosets are mainly governed by the cure condition, epoxy/anhydride ratio, and the composition (e.g., resin, curing agent and catalyst). It is believed that these factors must be controlled in order to tailor the mechanical and thermal properties of the ESO thermosets through networks with different crosslink densities and molecular structures.

### **2.2.3 Recent Development of Epoxidized Soybean Oil**

The ESO thermosets derived from biological origin substances have been recognized to be one of the new sustainable biopolymers today offering numerous environmental advantages, for example, they are readily biodegradable during polymer degradation process. However, the major problems encountered with the ESO thermosets are due to their inferior mechanical, thermal and thermo-physical properties(ref. Section 1.2). This is due to the low crosslink density and flexibility of the backbone structure in ESO. In this respect, some attempts have been made to improve these properties. The common used approaches were to prepare the blends and composites from ESO.

### 2.2.3.1 Epoxidized Soybean Oil-based Thermoset Blends

Ratna (2001) studied the mechanical and thermal properties of the unmodified ESO/diglycidyl ether of bisphenol-A (DGEBA) (blends of epoxy resins and ESO in a one-stage process) and the modified ESO/DGEBA blends (blends of epoxy resins and ESO in a two-stage process). It was found that the modified blends exhibited two distinct  $T_g$ , whereas the unmodified system displayed a sole  $T_g$  which was lower than the modified blends. The increase in ESO loading did not improve the impact strength of the unmodified ESO system to a satisfactory level. In contrast, the impact strength of modified blends improved 26% with the addition of 20 phr ESO resin.

Park et al. (2004) reported the mechanical and thermal properties of ESO/4,4-tetradiglycidyl diaminodiphenol methane (TGDDM) blends cured with the diamino-diphenyl methane amine (DDM) hardener. DSC thermograms showed that the peak maximum temperature of the ESO/TGDDM blends shifted to higher temperatures by increasing the ESO loading. DMA spectra of ESO/TGDDM blends, which displayed a single relaxation, proved that the ESO resin was miscible with the TGDDM resin. Fracture toughness and flexural strength of the ESO/TGDDM also improved linearly by increasing the ESO loading from 0 to 10 wt%. This could be explained in terms of the addition of larger molecular weight ESO into the TGDDM resin, resulting to a decrease in elastic modulus of the ESO/TGDDM blends.

Miyagawa et al. (2005) investigated the thermophysical and impact properties of the ESO/diglycidyl ether of bisphenol-F (DGEBF) blends cured with methyltetrahydrophthalic anhydride in the presence of 1-methylimidazole catalyst. It was reported that the storage modulus and  $T_g$  of the ESO/DGEBF blends decreased approximately 20% and 7–9%, respectively, after blending with 30–50 wt% of ESO resin. Also, the crosslink density of ESO/DGEBF blends reduced slightly when 30 wt% of ESO was

blended with DGEBF resin. However, the impact strength and fracture toughness of ESO/DGEBF blends improved significantly with the addition of ESO. The possible toughening mechanism of ESO/DGEBF blends was attributed to the phase separation of the ESO and DGEBF resins. This is attributed to the fact that the presence of the second phase of ESO rubbery particles into the DGEBF matrix enhanced the plastic deformation and subsequently added a significant amount of fracture energy to the crack propagation process.

Yue et al. (2007) determined the effect of the ESO loading on the mechanical properties of ESO/phenolic blends with different catalysts (i.e., a mixture of tertiary amine, a mixture of multi-amine, or a mixture of catalysts). The experimental results showed that the flexural strength and the toughening effects of ESO/phenolic blends with tertiary amine and multi-amine were superior to other modified phenolic resins with ESO content up to approximately 30% and 40%, respectively.

Jin & Park (2008a) studied the influences of ESO compositions on the impact and adhesive strength of ESO/DGEBA blends. Taking advantage of the flexibility of ESO, an improvement of 58% in the impact strength and an increment in adhesive lap shear strength were obtained when 60 wt% and 40 wt% of the ESO resins was blended into ESO/DGEBA systems, respectively. Jin & Park (2008b) also reported that ESO/DGEBA blends showed two DSC exotherm peaks. This implied a complex behaviour of possible multiple curing reactions. However, the ESO/DGEBA blends showed a high degree of homogeneity since the blends exhibited a single relaxation intermediate peak between the pristine ESO and DGEBA components.

Altuna et al. (2011) reported the effects of ESO resin on the compression and optical properties of the ESO/DGEBA blends. The blends with a higher ESO content possessed lower compressive yield strength and compressive modulus. The scanning